Proceedings of ASME Turbo Expo 2016: Turbomachinery Technical Conference and Exposition
GT2016
June 13 – 17, 2016, Seoul, South Korea

GT2016-57808

ANALYSIS OF FAN STAGE DESIGN ATTRIBUTES FOR BOUNDARY LAYER INGESTION

D. K. Hall, E. M. Greitzer, C. S. Tan
Gas Turbine Laboratory
Department of Aeronautics and Astronautics
Massachusetts Institute of Technology
Cambridge, Massachusetts 02139
Email: dkhall@mit.edu

ABSTRACT

This paper describes a new conceptual framework for three-dimensional turbomachinery flow analysis and its use to assess fan stage attributes for mitigating adverse effects of inlet distortion due to boundary layer ingestion (BLI). A non-axisymmetric throughflow method has been developed to describe the fan flow field with inlet distortion. In this the turbomachinery is modeled using momentum and energy source distributions that are determined as a function of local flow conditions and a specified blade camber surface geometry. Comparison with higher-fidelity computational and experimental results shows that the method captures the principal flow redistribution and distortion transfer effects associated with BLI. Distortion response is assessed for a range of (i) rotor spanwise work profiles, (ii) rotor-stator spacings, and (iii) non-axisymmetric stator geometries. For the parameters examined, changes in axisymmetric design result in trades between rotor and stator distortions, or between different radial sections of a given blade row with marginal overall gain. Of the approaches examined, non-axisymmetric stator exit flow angle distributions were found to provide the greatest reduction in rotor flow distortion and thus may offer the most potential for mitigating decreases in performance due to BLI inlet distortion.

INTRODUCTION

In this paper we present an analysis of fan stage behavior with inlet distortion from boundary layer ingestion (BLI). As has long been known, BLI, i.e., having a portion of an aircraft's boundary layer pass through the propulsor, and thus adding propulsive power to the flow at a lower average velocity, decreases the excess kinetic energy in the downstream jet and increases propulsive efficiency, potentially reducing aircraft fuel burn [1–4]. Two recent BLI aircraft concepts are the Cambridge-MIT Silent Aircraft [5], and the D8 "double bubble" aircraft, which was developed as part of the NASA N+3 research program to reduce environmental impacts of aviation [6, 7]. The D8 has also been assessed in low speed wind tunnel experiments, where direct comparison of powered models in BLI and non-BLI configurations showed the former gave reductions in required propulsive power of up to 10% [8]. A challenge presented by BLI, however, is the non-uniform stagnation pressure (i.e., stagnation pressure distortion) entering the propulsion system, with the possibility of decreased component efficiency, reduced fan and compressor stall margin, and increased unsteady forces on rotating turbomachinery.

The aerodynamic response of propulsors to inlet distortion has received much attention; an introductory review is given by Longley and Greitzer [9]. Fans and compressors attenuate stagnation pressure distortions, with increased attenuation associated with steeper slopes of the pressure rise versus flow characteristics. Other relevant features include the upstream circumferential flow redistribution that accompanies this attenuation, and the strong interactions between rotor, stator, and downstream components due to the longer (radius scale) interaction lengths. These effects have been well-described for two-dimensional flows [10, 11], and some of the ideas will be used

here to give insight into the response to BLI distortion. It will be seen, however, that there are features in low hub-to-tip ratio machines that require a three-dimensional flow description.

There has been recent computational work on BLI fan stage performance, including design of a distortion-tolerant BLI fan stage, where the design estimates are for reductions in stage efficiency of 1-2% relative to uniform inlet flow [12]. Other computational and experimental analyses have found similar efficiency reductions for different geometries [13, 14]. Gunn and Hall have illustrated that fan stage performance depends strongly on three-dimensional flow redistributions upstream of the fan and through the rotor, and that stage efficiency is linked to circumferential flow non-uniformities, particularly in local diffusion factor [14]. A useful finding from comparison of calculations for incompressible and transonic flow is that although the details of the flow change (e.g, the occurence of shocks in the latter regime), the overall features of flow redistribution that determine changes in stage efficiency with inlet distortion are not sensitive to Mach number.

The objective of the present work is to determine fan stage attributes that mitigate the effects of inlet distortion on performance. Vertically stratified stagnation pressure distributions representative of inlet distortion for BLI aircraft with short, low-offset inlets such as the D8 [7] are considered. The analytical framework described, however, can be applied to a variety of non-axisymmetric turbomachinery flow distortions [15]. The focus is on *design point aerodynamic efficiency*; stability and aeromechanics are mentioned in passing but are beyond the scope of this paper. We emphasize that the problem is treated at the *conceptual level*, which includes the specification of design point flow coefficient and spanwise distribution of stagnation enthalpy rise coefficient (i.e., velocity triangles), axial location of the rotor and stator, and mean camber line. In other words, knowledge of blade profile, which is obtained later in the design process, is not required. In this context, we emphasize that the intent is not to develop a design methodology for BLI propulsors, but rather *to identify conceptual design attributes* that provide favorable conditions for fan stage operation with distortion.

We assess the effect of design choices on BLI fan performance from flow field behavior using a newly developed non-axisymmetric turbomachinery throughflow method. The basic idea is to replace the three-dimensional blade geometry with momentum and energy source distributions that generate the flow turning and pressure rise of the turbomachinery [16]. Such methods have been used to assess the effect of flow non-uniformities on multistage compressor stability [17], fan aerodynamic performance [18], and fan aeroacoustics [19]. Unlike these previous methods, however, in which the source distributions are extracted from single passage flow solutions, in the current approach the sources are determined as a function of local flow conditions and an approximate blade geometry, so *a priori* flow calculations are not needed. The flow is taken to be inviscid, which is appropriate because, as will be seen, the mechanisms that determine the fan distortion response are inviscid. Further, inviscid blade performance metrics such as diffusion factor can be used as surrogates for efficiency. The model flow is also taken to be incompressible, which simplifies the analysis and is appropriate in light of the findings of Gunn and Hall [14] regarding the insensitivity of flow redistribution effects to Mach number.

The paper is organized as follows. We first provide a description of the non-axisymmetric throughflow methodology. We then apply the analysis to a fan with BLI inlet distortion and present comparisons with results of higher-fidelity calculations and experiments. These show the degree to which the relevant distortion-fan interactions are captured. Third, we determine the effectiveness of different design features by assessing their impact on the magnitude of circumferential flow non-uniformities. Finally, based on these results, we discuss those attributes that have the greatest potential to mitigate the impact of BLI inlet distortion on fan stage performance.

NON-AXISYMMETRIC THROUGHFLOW METHOD

In this section, we describe the three-dimensional analysis of turbomachinery blade row response to flow distortions. For clarity, the basic concept is illustrated in two dimensions only in Fig. 1, which shows the actual flow and its representation by the equivalent model flow. In the latter, the bladed region is replaced with an axisymmetric fluid volume over the meridional extent of the blade row, within which are momentum and energy source distributions to generate flow turning, pressure rise, and enthalpy rise representative of that produced by the actual geometry, in a pitchwise-averaged sense. The source distributions are defined as a function of local flow conditions and a specified blade camber surface geometry. For uniform inlet con-

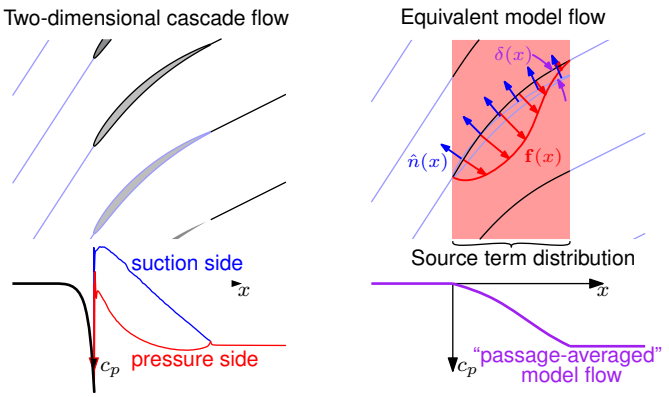

FIGURE 1. COMPARISON OF TWO-DIMENSIONAL CASCADE FLOW TO EQUIVALENT MODEL FLOW WITH SOURCE DISTRIBUTION

ditions, the source distribution generates an axisymmetric flow field equivalent to the circumferential average of the actual flow. For non-axisymmetric flow, the source distribution is circumferentially non-uniform and generates the appropriate distortion transfer across the blade row.

Source Term Formulation

Equations of Motion. The description here is presented in terms of inviscid flow. There is no bar to including viscous effects, but it will be seen that an inviscid description is adequate to capture the relevant flow mechanisms for the problem of interest. For steady flow, the local momentum and energy source terms are represented as a body force per unit mass $\mathbf{f}$ and an energy addition rate per unit mass $\dot{e}$. The equations of conservation of mass, momentum, and energy, including the source terms, are,

$$\nabla \cdot (\rho \mathbf{V}) = 0, \tag{1}$$

$$\mathbf{V} \cdot \nabla \mathbf{V} + \frac{1}{\rho} \nabla p = \mathbf{f}, \tag{2}$$

$$\mathbf{V} \cdot \nabla h_t = \mathbf{V} \cdot \mathbf{f} + \dot{e}. \tag{3}$$

Equations (1) and (2) are sufficient to describe an incompressible flow field, but the general compressible case including Eq. (3) is considered to examine the relationship between the source terms and the stagnation enthalpy and entropy, corresponding to work addition and losses, respectively. The stagnation enthalpy change along a streamline is zero except in rotating blade rows, where it corresponds to changes in swirl velocity due to the circumferential force,

$$\mathbf{V} \cdot \nabla h_t = (\Omega r) f_\theta. \tag{4}$$

Equation (4) is the differential form of the Euler turbine equation for the model flow. The energy source, $\dot{e}$, corresponds to entropy generation in the model flow

$$T \mathbf{V} \cdot \nabla s = \dot{e}. \tag{5}$$

Combining Eqs. (3)-(5), the entropy generation is related to the body force component in the relative streamwise direction,

$$T \mathbf{V} \cdot \nabla s = -\mathbf{W} \cdot \mathbf{f}, \tag{6}$$

where $\mathbf{W} = \mathbf{V} - (\Omega r)\hat{\theta}$ is the blade-relative velocity.

Equation (6) shows the usefulness of characterizing the momentum source in terms of components parallel and normal to the relative direction. Entropy is generated in the model flow by a force, f_ℓ, acting opposite the streamwise direction in the relative frame, combined with the energy source, $\dot{e}$ [20]. The force normal to the relative flow direction, f_n, generates reversible flow turning. Near the design point of axial turbomachines, the contribution of f_ℓ to flow turning, pressure rise, and enthalpy rise is much smaller than f_n, and we neglect it in the current description, consistent with the assumption of inviscid flow.

Blade Loading Model. The source term distribution is defined as a function of local flow conditions and an approximate blade geometry, characterized at this conceptual stage by a blade camber surface normal distribution, $\hat{\mathbf{n}}(x, r)$. Figure 1 shows the normals in a two-dimensional representation, in which they vary in the axial direction only and define the local blade metal angle. In three dimensions, the normal vector also has a radial component associated with blade twist and lean.

The normal momentum source per unit mass, f_n, is modeled as a blade force that scales with the local deviation angle δ between the blade tangent surface and the relative velocity vector, distributed uniformly over one blade pitch,

$$f_n = \frac{(2\pi\delta)\left(\frac{1}{2}W^2/|n_\theta|\right)}{2\pi r/B} \tag{7}$$

The constant 2π in Eq. (7) yields flat plate airfoil lift ($c_\ell = 2\pi\delta$) in the low solidity ($s/c \to \infty$) limit, and in the high solidity ($s/c \to 0$) limit, the flow is everywhere tangent ($\delta = 0$) to the blade camber surface. The direction of f_n is normal to the relative streamwise direction and in the plane shared by the local blade normal $\hat{\mathbf{n}}$ and the relative velocity vector, $\mathbf{W}$. The normal force thus acts to reduce the local deviation, δ, between relative velocity and blade surface.

Equation (7), plus the geometric constraints on the direction of momentum source vector, provide closed form expressions for the source terms as a function of the local flow conditions and specified camber surface normal geometry. The flow field is determined using conventional steady CFD techniques, including momentum and energy sources, which are calculated iteratively as a function of the local velocity as the simulation converges to a solution that satisfies the equations of motion including the sources.

Assumptions and Applicability of the Analysis

The throughflow method includes several simplifying assumptions which we now describe in terms of interpreting the results. One is that the flow is locally quasi-axisymmetric, in other words, that f_n depends on the local flow conditions, but not on gradients in the circumferential direction. The assumption is appropriate if the characteristic length scale of circumferential non-uniformities is much larger than the blade pitch. This

is the case for the geometries considered, which have 20 or more blades, and for BLI inlet distortions whose circumferential length scale is the radius.

A related implication of the circumferential distortion length scale is that unsteadiness in the blade-relative frame can be neglected. The importance of unsteady effects is implied by the reduced frequency, β, which relates the time scales of the flow unsteadiness and the passage throughflow. For distortions with characteristic length scale equal to the radius, β can be approximated in terms of the rotor geometry,

$$\beta = \frac{(c_x/V_x)}{(2\pi/\Omega)} \approx \frac{(\cos\xi)(1 - r_{\rm hub}/r_{\rm tip})}{2\pi\phi AR} \tag{8}$$

where ϕ is the flow coefficient, ξ is the blade stagger, $r_{\rm hub}/r_{\rm tip}$ is the blade hub-to-tip ratio, and AR is the blade aspect ratio. For the fan stage geometries considered here, $\beta < 0.1$, and the flow is assumed to be quasi-steady. Comparison of a source distribution method with full-wheel unsteady (URANS) calculations has shown fan distortion response to be well represented by this sort of flow description [18].

Because we describe the flow in a passage-averaged sense, blade-to-blade features, such as boundary layers, wakes, secondary flows, and tip clearance flow structures, are not resolved. In addition, as mentioned previously, because the interest is in behavior near the fan design point, the flow is taken as inviscid, and blade and end wall losses are not included. These can be added (e.g., non-zero f_ℓ and $\dot{e}$ terms to capture the effect of blade losses), but they are not necessary to capture the inviscid redistribution effects that dominate the non-uniform flows examined, as will be seen in the next section.

In summary, the framework we present provides a means of estimating fan stage distortion response without a detailed blade design or use of full-wheel URANS calculations. The assumption of quasi-steady flow means steady CFD techniques can be used. Further, the source distribution description and assumption of inviscid flow mean solutions can be obtained using a relatively coarse grid on an axisymmetric computational domain (i.e., a body of revolution obtained by revolving the meridional flowpath about the centerline) without resolving the blade-to-blade geometry or end wall boundary layers. The main benefit of the method, however, is not these reductions in computational cost, but rather the capability to assess the impact of various stage design parameters on propulsor performance before detailed blade design is carried out. This is achieved by using approximate, parametrically defined camber surface distributions which allow manipulation of the radial variations in stage velocity triangles at the (uniform inlet) design point. The combination of parametrically defined blading geometry and low computational cost makes the method well-suited to conceptual level parametric analysis of distortion response with changes in fan stage design.

FAN STAGE DISTORTION RESPONSE

In this section we analyze fan stage flow fields with and without distortion using the non-axisymmetric throughflow method we have described. There are two objectives. One is to show, based on comparison of the results with experimental data and with higher fidelity computations, the approximations capture the behavior of fan response to BLI distortion. The second is to identify and describe the features of the relevant flow non-uniformities within the blade rows and the mechanisms through which they effect blade row performance. These mechanisms and their sensitivity to fan stage design choices, are considered in the next section.

Whittle Laboratory BLI Fan Rig

The geometry examined is the low speed fan stage used in the experiments of Gunn, Tooze, Hall, and Colin [13], Gunn and Hall [14], and Perovic, Hall, and Gunn [21] to assess fan stage response to inlet distortion. Design parameters of the fan are listed in Table 1, and a meridional view of the fan stage geometry, computational domain, and the axial measurement planes is given in Fig. 2. The domain extends approximately two diameters upstream of the spinner tip and downstream of the stator trailing edge. Rotor and stator camber distributions are estimated based on radial distributions of leading and trailing edge metal angles [22].

The domain was meshed using Pointwise [23]. Axisymmetric flow calculations were carried out on a 22.5° wedge domain with circumferentially periodic boundary conditions and a but-

TABLE 1. WHITTLE BLI FAN RIG DESIGN PARAMETERS

Flow coefficient, $= \dot{m}/(\rho A_1 U_{\rm mid})$	0.5
Stage work coefficient, $= \Delta h_t/U^2_{\rm mid}$	0.47
Stage reaction	0.81
Rotor inlet tip Mach number	0.13
Rotor tip Reynolds number	2.0×10^5
Rotor inlet hub-to-tip radius ratio	0.3
Rotor inlet tip diameter	0.5 m
Number of rotor blades	20
Number of stator vanes	30

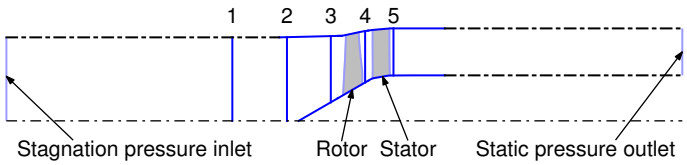

FIGURE 2. MERIDIONAL GEOMETRY OF WHITTLE BLI RIG COMPUTATIONAL DOMAIN

terfly mesh upstream of the spinner. The full-wheel grid consisted of 16 copies of the the wedge domain. Grid converged results were obtained using 1.8 million cells for the full-wheel grid. Calculations were performed with ANSYS CFX, a finite volume solver, using the built-in "high resolution" discretization scheme [24]. Inviscid flow was modeled by solving the laminar Navier-Stokes equations with zero viscosity and slip wall boundary conditions on the hub and casing. The inlet stagnation pressure was fixed with flow normal to the inlet boundary. The rotor velocity corresponded to a rotor tip Mach number of 0.13. The fan operating point was set by varying the outlet static pressure.

Figure 3 shows a comparison of calculated and measured stage stagnation pressure rise characteristic, as well as the design point stagnation enthalpy rise. The inviscid approximation does not include blade losses, and the stagnation pressure rise and stagnation enthalpy rise coefficients are equivalent. The calculations match the measured stage loading coefficient to within 3% at the design point flow coefficient, $\dot{m}/(\rho A_1 U_{\mathrm{mid}}) = 0.5$.

Figure 4 shows spanwise distributions of pitchwise-averaged rotor inlet and exit axial velocity at the stage design point. Model and measurements agree well over most of the blade span. Near the endwalls, the model does not capture the effect of rotor tip clearance and endwall boundary layers, but those discrepancies do not have a large impact on the mean flow. Further, as will be seen, the throughflow method still captures the flow *non-uniformities* near the endwalls with inlet distortion.

BLI Inlet Distortion

As a reference for estimates of the effect of inlet distortion on fan stage behavior, the throughflow method has been applied to the distortion experiments of Gunn and Hall [14]. The inlet stagnation pressure distribution is shown in Fig. 5. The vertically stratified distribution is representative of BLI distortion for the aircraft of interest, which has embedded propulsors with small offset from the fuselage surface and short inlets [7]. There are small (compared to a radius) length-scale variations in the stagnation pressure distribution due to the design of the screen used in the experiments to generate the distortion. For consistency in comparison of the measurements and calculations, these variations are included in the specification of the inlet boundary conditions for the latter.

Rotor Flow Field

The conditions at the rotor inlet are set by the upstream redistribution due to interaction between the inlet distortion and the fan. Because of the difference in local pressure rise across the fan and the (approximately) circumferentially uniform stage exit static pressure, low stagnation pressure streamtubes experience greater streamwise acceleration upstream of the fan. The consequences are (i) attenuation of the axial velocity distortion, (ii) a top-to-bottom flow redistribution due to larger streamtube contraction of the low stagnation pressure flow, and (iii) angular velocity distortions at the rotor inlet.

Figure 6 shows a comparison of calculated and measured circumferential distributions of rotor inlet (station 3) axial velocity and absolute swirl angle, at 25% and 75% span, at the design point flow coefficient of the fan stage of Gunn and Hall [14]. The small length-scale inlet stagnation pressure variations due to the screen design convect downstream to the rotor inlet, resulting in

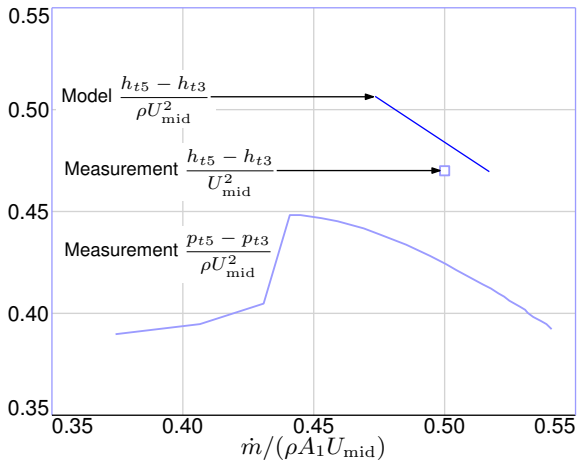

FIGURE 3. STAGNATION PRESSURES RISE CHARACTERISTIC WITH UNIFORM INLET CONDITIONS; COMPARISON OF THROUGHFLOW METHOD AND MEASUREMENTS [14]

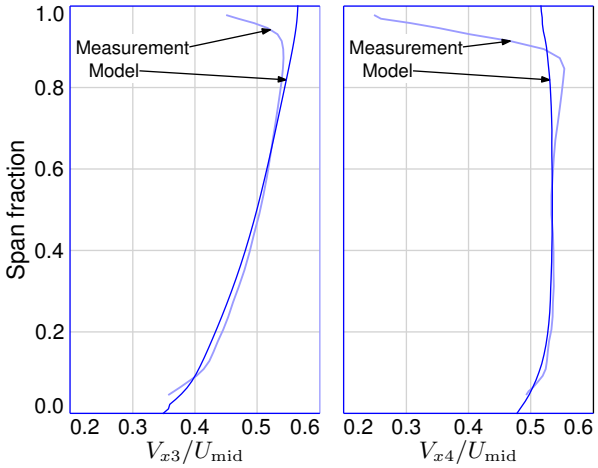

FIGURE 4. SPANWISE DISTRIBUTIONS OF AXIAL VELOCITY NORMALIZED BY MIDSPAN WHEEL SPEED UPSTREAM AND DOWNSTREAM OF THE ROTOR; COMPARISON OF THROUGHFLOW METOHD AND MEASUREMENTS [14]

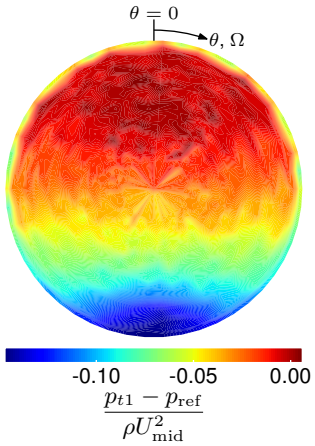

FIGURE 5. MEASURED INLET STAGNATION PRESSURE DISTRIBUTION [22]

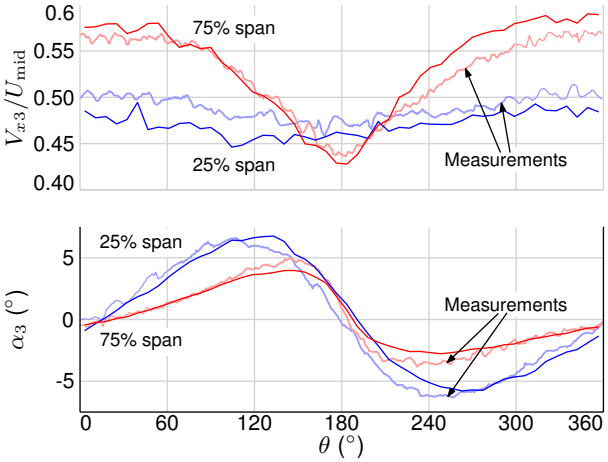

FIGURE 6. CIRCUMFERENTIAL DISTRIBUTIONS OF ROTOR INLET AXIAL VELOCITY AND ABSOLUTE SWIRL ANGLE; COMPARISON OF THROUGHFLOW METHOD AND MEASUREMENTS [14]

the rippled velocity distributions observed in both the calculation and measurements. The screen-created variations are negligible compared to the peak-to-peak distortion magnitude. Further, the coarse grid resolution relative to these perturbations filters out the higher harmonic content in the calculations.

The axial velocity distortion is larger near the tip than near the hub, because of the spanwise variation in stagnation pressure circumferential non-uniformity. The absolute swirl angles are largest at circumferential locations near $\theta = 90°$ and $\theta = 270°$ (measured from $\theta = 0°$ at the top of the fan, so the peak upstream stagnation pressure distortion occurs at $\theta = 180°$), where the downward component of the velocity is aligned with the circumferential direction, and near the hub, where the downward velocity is increased due to the blockage of the spinner. The difference in axial velocity distortion between the two spans, as well as the shapes of the circumferential distributions, is well captured. The flow far upstream is axial, and the measured rotor inlet swirl, and thus the upstream redistribution, is also captured by the throughflow method.

The upstream redistribution results in circumferential nonuniformities in rotor relative inlet flow angle, stagnation enthalpy rise, streamtube contraction, and diffusion through the rotor, as illustrated in Fig. 7. Figure 7a shows the difference between calculated rotor inlet relative flow angle, β_3, and the circumferential average at that radius, which represents the local incidence angle distortion. For a tip section, the inlet flow angle reaches a maximum near $\theta = 180°$, where the stagnation pressure and axial velocity are low and the absolute swirl angle is near zero (the region labeled A in Fig. 7). For a hub section, the axial velocity distortion is small, and the main impact on incidence angle is the decrease due to co-swirl (at B) and increase due to counter-swirl (at C). At midspan, variations in both axial and swirl velocity affect the local incidence, but the flow angle distortions are smaller than those near the hub and tip. The peak-to-peak circumferential nonuniformity in incidence angle is largest at the hub, even though the incoming stagnation pressure distortion is smallest there.

Figure 7b shows the rotor stagnation enthalpy rise coefficient distribution. The work input exhibits circumferential nonuniformities similar to the incoming relative flow angle shown in Fig. 7a, indicating circumferential variations in incidence angle, and thus flow turning, have a larger effect on work input than velocity non-uniformities. The peak stagnation enthalpy rise occurs at the location of peak rotor tip incidence near region A. The hub has the lowest loading for uniform inlet conditions, and it experiences decreased loading (relative to the circumferential mean) near $\theta = 90°$, where the hub incidence is most negative, and increased loading near $\theta = 270°$, where the hub incidence is largest, due to the swirl distortion seen at B and C in Fig. 7a.

The non-uniform work input results in non-uniform streamtube contraction through the blade row, shown in Fig. 7c. The contraction is larger where the work input is high (region D). This is consistent with observations by Gunn and Hall [14] of radial redistribution between rotor inlet and exit that reduces the axial velocity distortion.

Figure 7d shows local diffusion factor, defined on a streamline from rotor inlet to exit,

$$D = 1 - \frac{W_{\mathrm{out}}}{W_{\mathrm{in}}} + \frac{|r_{\mathrm{out}} W_{\theta \mathrm{out}} - r_{\mathrm{in}} W_{\theta \mathrm{in}}|}{W_{\mathrm{in}}} \frac{2\pi/B}{c_{\mathrm{ref}}}, \qquad (9)$$

where c_{ref} is a reference chord length and B is the number

of blades or vanes. The throughflow method captures two effects linked to experimentally observed changes in local rotor blade performance. First, the large streamtube contraction near $\theta = 180°$ results in a local decrease in diffusion factor, even with large flow turning (at E). Second, the circumferential non-uniformity in diffusion factor is largest near the tip, and the peak diffusion factor in the tip region occurs to the left of the $\theta = 180°$ position (at F). In the actual flow, this increased loading results in a separation that continues around a large portion of the annulus [14]. The approximate analysis does not resolve this feature, but the circumferential variations in diffusion factor are consistent with experimental results [14], and regions of peak diffusion factor appear to be good indicators of the potential separation locations in the actual flow. The magnitude of the diffusion factor circumferential distortion is therefore used in the next section as a metric to characterize non-uniformity in local blade conditions.

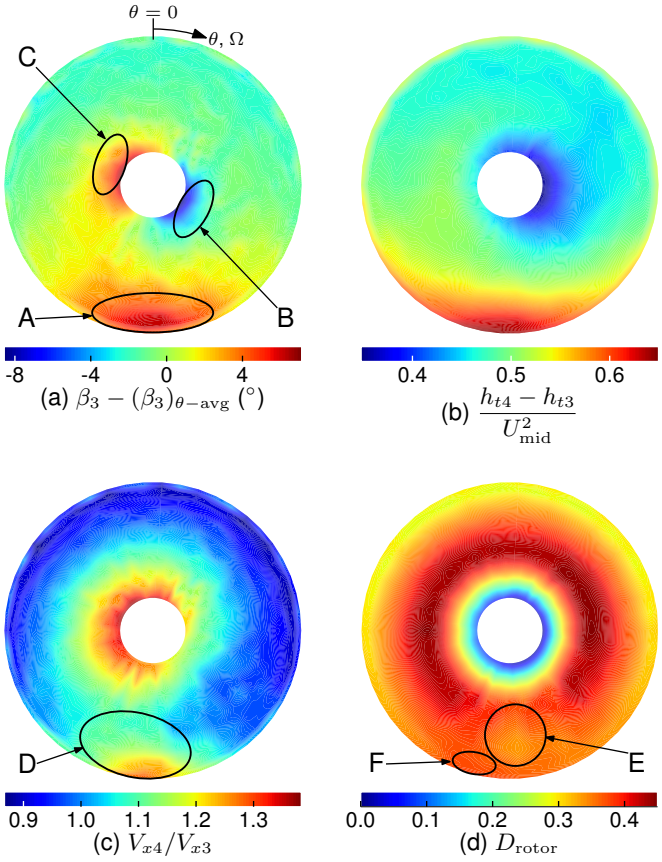

FIGURE 7. ROTOR INLET RELATIVE FLOW ANGLE DISTORTION (a), STAGNATION ENTHALPY RISE (b), STREAMTUBE CONTRACTION (c), AND DIFFUSION FACTOR (d)

Stator Flow Field

Figure 8 shows a comparison of calculated and measured circumferential distributions of stator inlet (station 4) axial velocity and absolute swirl angle, at 25% and 75% span. Comparison with Fig. 6 shows that both radial and circumferential variations in axial velocity are smaller at rotor exit than at rotor inlet. The calculated axial velocity distortion is in good agreement with the measurements. The swirl angle distribution also agrees with the data, but the absolute swirl magnitudes are overestimated by approximately 5°. This is most likely due to the blade loading model (Eq. (7)) underestimating the trailing edge deviation, which is also consistent with the slight overprediction of the design point stage loading coefficient. The agreement with experimental measurements in Figs. 6 and 8 demonstrates that the throughflow method captures the important aspects of the three-dimensional flow redistribution and rotor distortion response behaviors. It can therefore be used to determine the magnitude of circumferential flow non-uniformities and to assess blade row performance with BLI distortion.

Figure 9 shows distributions of stator inlet stagnation pressure, axial velocity, swirl angle, and stator diffusion factor. The stagnation pressure distribution, shown in Fig. 9a, results from the combination of the far upstream inlet distortion and the non-uniform work input (Fig. 7b). The smallest circumferential variation in stagnation pressure is near the tip, where the non-uniformity in rotor work input is large. At midspan, there is low stagnation pressure to the right of $\theta = 180°$ (at A) where the incoming stagnation pressure is low and the rotor pressure rise is reduced due to co-swirl. The largest circumferential variation

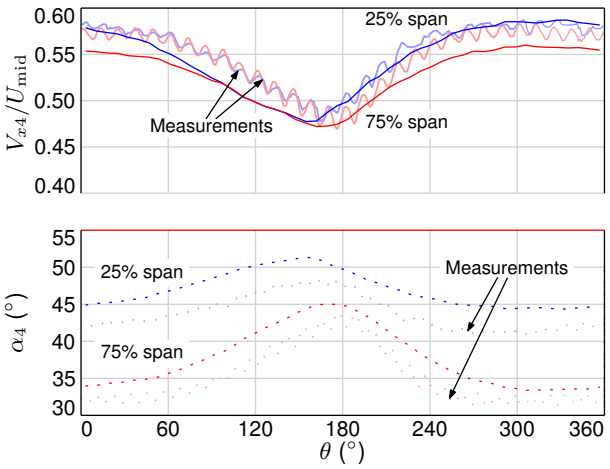

FIGURE 8. CIRCUMFERENTIAL DISTRIBUTIONS OF STATOR INLET AXIAL VELOCITY AND ABSOLUTE SWIRL ANGLE; COMPARISON OF THROUGHFLOW METHOD AND MEASUREMENTS [14]

in stagnation pressure is near the hub, where even though the upstream distortion is low, the rotor incidence range, and thus non-uniformity in rotor pressure rise is large. This may be of concern for the stability of downstream compressors, which typically ingest the rotor exit hub flow, although that issue is beyond the scope of this paper.

The rotor exit axial velocity distortion, shown in Fig. 9b, is reduced relative to that at rotor inlet. The lowest axial velocities occur to the right of $\theta = 180°$ (at B), where upstream velocity is low, and pressure rise and distortion attenuation through the rotor are reduced due to co-swirl. The rotor exit flow angle is approximately uniform, so the absolute swirl angle, shown in Fig. 9c, is increased in the region of decreased axial velocity.

The largest effect on stator diffusion factor, Fig. 9d, is that of flow turning, and the diffusion factor is thus increased in the region of decreased axial velocity, where the incoming swirl angle is largest. Peak diffusion factor and the largest circumferential variation in diffusion factor both occur near the hub, consistent with the observations of Gunn and Hall [14], where the increased loading was seen to lead to hub corner separation near the location of highest diffusion (at C). Again, separation is not captured by the approximate analysis, but circumferential variation in diffusion factor appears to be a good predictor of regions of increased blade loss.

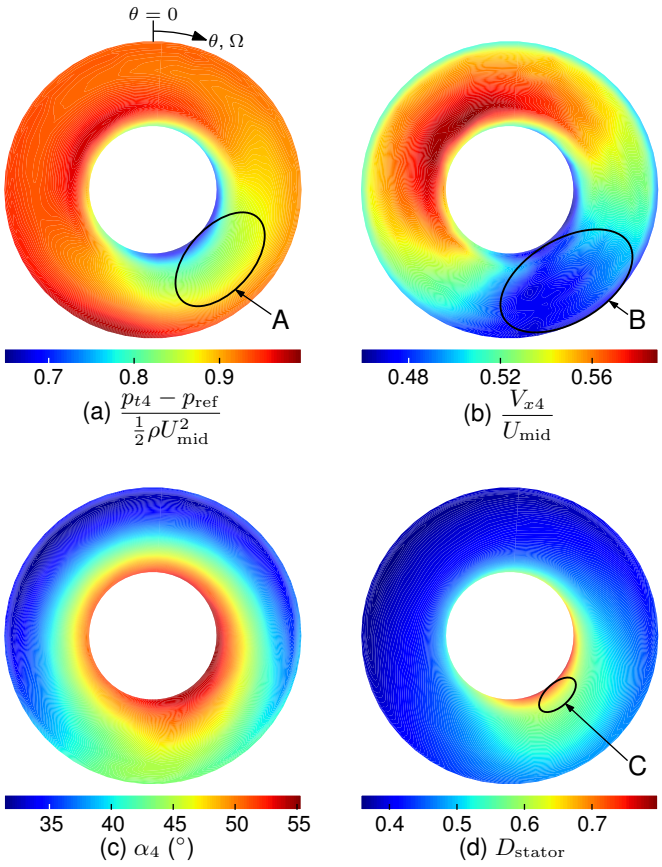

FIGURE 9. STATOR INLET AXIAL STAGNATION PRESSURE (a), INLET AXIAL VELOCITY (b), INLET ABSOLUTE SWIRL ANGLE (b), AND DIFFUSION FACTOR (d)

EFFECT OF TURBOMACHINERY DESIGN

The information in the previous section shows that the throughflow method captures both the three-dimensional flow redistribution and the resulting flow non-uniformities that drive changes in fan efficiency with BLI. We therefore now examine the effect of stage design features on these flow mechanisms and blade performance. The fan stages examined are based on the NASA R4 fan stage, which has a design pressure ratio (1.47) and hub-to-tip ratio (0.3) representative of contemporary fan stages. The performance with uniform inlet conditions is documented reference [25]. A meridional cut of the flowpath geometry is given in Fig. 10.

The inlet stagnation pressure distribution of Fig. 11, was used as input. This distribution was based on computed propulsor inlet conditions for a 1:11 scale wind tunnel model of the D8 aircraft with BLI [26]. The overall features of the inlet stagnation pressure distribution are similar to those in the previous section, but the distribution in Fig. 11 is explicitly linked to the aircraft of interest.

The impact of (i) axial location of the downstream stator, (ii) stage design point flow coefficient and stagnation enthalpy rise coefficient, (iii) radial distribution of stagnation enthalpy rise, and (iv) non-axisymmetric stator exit flow angle were examined. The axial stator locations are seen in Fig. 10. Figure 12 shows the (axisymmetric flow) design point loading and flow coefficients for the five geometries assessed. All the designs have constant ψ/ϕ^2, representing the condition of constant thrust, which is the relevant comparison. Figure 12 also shows the spanwise distribution of stagnation enthalpy rise for the five rotor geometries. Uniform radial work distribution designs at different stage design points are compared to assess the effect of pressure rise characteristic slope, which increases in steepness with decreasing ϕ and

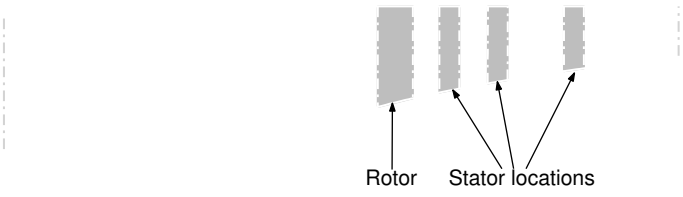

FIGURE 10. MERIDIONAL GEOMETRY OF FAN STAGE DOMAIN FOR DESIGN SENSITIVITY STUDY, WITH THREE AXIAL STATOR LOCATIONS SHOWN

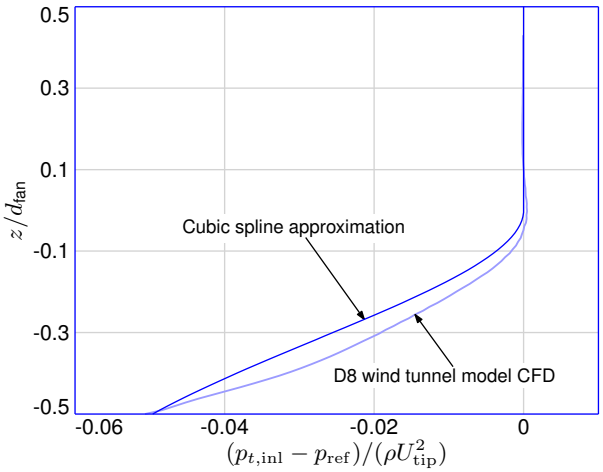

FIGURE 11. INLET STAGNATION PRESSURE DISTRIBUTIONS: CUBIC BOUNDARY LAYER VELOCITY FITS OF COMPUTED WIND TUNNEL MODEL BLI AIRCRAFT PROPULSOR

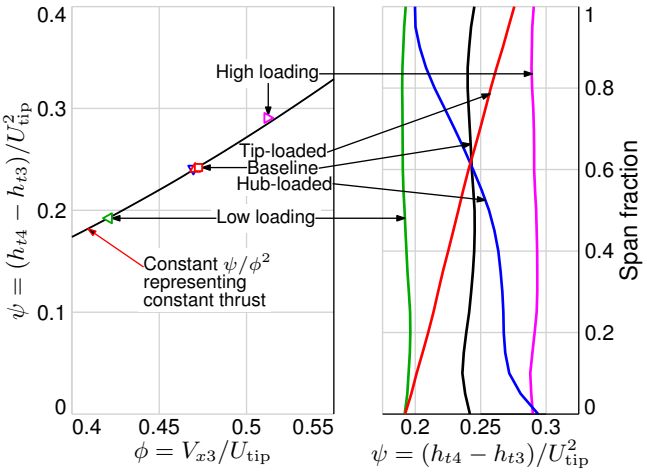

FIGURE 12. STAGE AXISYMMETRIC FLOW DESIGN POINT FLOW AND STAGNATION ENTHALPY RISE COEFFICIENT, AND RADIAL STAGNATION ENTHALPY RISE DISTRIBUTION FOR DIFFERENT ROTOR DESIGNS

ψ. Different radial work distributions at fixed stage loading and flow coefficient are compared to assess the effect of local variations in rotor loading.

The rotor camber normal distributions were generated by fixing the inlet metal angle distribution for zero incidence based on design point flow coefficient, using circular arc camber distributions at a given spanwise section, and adjusting the exit metal angle distribution until the desired enthalpy rise was achieved. The baseline stator camber surface was taken as a flat plate with zero stagger (i.e., $\hat{\mathbf{n}}_{\text{stator}} = \hat{\theta}$), because the distortion response is determined by the stator *exit flow angle* and does not depend on the details of the camber line. Non-axisymmetric stator exit flow angles were generated using a circumferential stator exit angle variation of the form,

$$\kappa_{\text{stator}}(\theta) = (\delta\kappa)\cos(\theta - \varphi_\kappa), \tag{10}$$

where $\delta\kappa$ and φ_κ define the magnitude and phase of the perturbation in stator exit metal angle.

The design variations are assessed using the *peak-to-peak* circumferential variation in *rotor and stator diffusion factor* as metrics. We first consider the impact of rotor design point loading distribution, then the impact of stator location and non-axisymmetry.

Effect of Rotor Loading Distribution

Figure 13 shows rotor and stator diffusion factor distortion versus span fraction for the five rotor loading distributions of Fig. 12 with the baseline stator location. The rotor diffusion near the hub and tip are similar for all rotor designs. Near midspan, there is increased diffusion factor distortion for the low loading design due to increased nonuniform streamtube contraction that reduces the local diffusion in the low diffusion (region D of Fig. 7d). This increase in flow non-uniformity at low loading is opposite to behavior expected from "parallel compressor" concepts, in which decreased loading and steeper pressure rise characteristic give more uniform velocities and less performance degradation [9]. As such, the behavior illustrates *the importance of three-dimensional redistribution*. The high loading design enables smaller circumferential nonuniformities in diffusion near midspan, but the price for this is a higher average diffusion factor.

For radial variations in rotor loading, at fixed design stage loading and flow coefficient, the upstream and rotor flow redistribution are similar to that with uniform loading. The local circumferential average and the peak-to-peak non-uniformity in diffusion factor at a given spanwise location increase with local loading. The overall three-dimensional redistribution behavior is thus governed by the stage loading and flow coefficient, although the local rotor diffusion factor distortion increases, and stator diffusion factor decreases, with increased local loading.

The non-uniformity in stator diffusion is increased as local rotor loading coefficient is reduced, although the effect is smaller than for the rotor midspan diffusion factor distortions just described. The local stator diffusion is determined by the rotor exit axial velocity; with the nearly constant rotor relative exit angle, smaller axial velocity gives larger turning, and thus higher diffusion, in the stator. The increase in stator diffusion distortion with

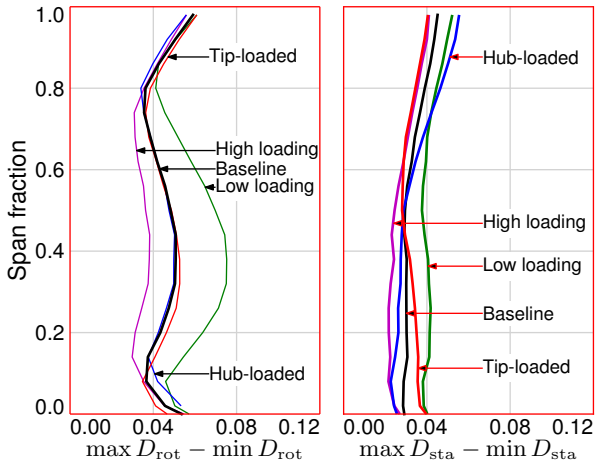

FIGURE 13. RADIAL DISTRIBUTIONS OF ROTOR AND STATOR DIFFUSION FACTOR DISTORTION MAGNITUDE FOR RADIAL STAGNATION ENTHALPY RISE DISTRIBUTIONS SHOWN IN FIG. 12

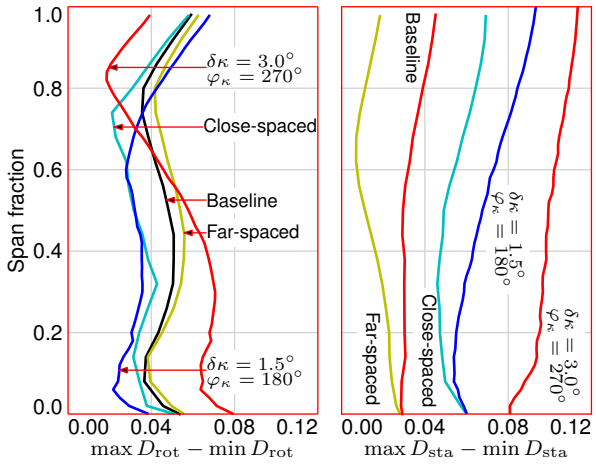

FIGURE 14. RADIAL DISTRIBUTIONS OF ROTOR AND STATOR DIFFUSION FACTOR DISTORTION MAGNITUDE FOR AXIAL STATOR LOCATIONS SHOWN IN FIG. 10 AND FOR NON-AXISYMMETRIC STATOR METAL ANGLE DISTRIBUTIONS

lower loading is thus a consequence of reduced rotor distortion attenuation.

Effect of Rotor-Stator Interaction

Figure 14 shows spanwise distributions of rotor and stator diffusion factor distortion for five stator designs. The baseline rotor loading distribution is used with three axisymmetric stator locations (Fig. 10) and two non-axisymmetric stator geometries at the baseline location. The latter were found to reduce rotor diffusion factor distortion locally near the hub and tip. The main finding is that changes in stator design can have a larger effect than the rotor work distribution on reducing diffusion factor distortion in either the rotor or stator. In all cases, however, reducing the non-uniformity in one blade row leads to increased distortion in the other. Decreasing rotor-stator spacing decreased the rotor distortion while increasing stator distortions, and non-axisymmetric stator exit angle distributions gave improvments in rotor diffusion factor over a portion of the span only while increasing stator distortion over the entire span.

The behavior of rotor and stator diffusion factor distortion can be explained in terms of the effect of stator design on rotor exit static pressure perturbations. This is illustrated conceptually in Fig. 15, which shows an "unrolled" two-dimensional flow representation of a spanwise section of the fan stage in the x-θ plane. To simplify the analysis (for this example only), we treat the rotor stagnation-to-static pressure as a function of rotor inlet axial velocity. If the rotor exit static pressure distortion is the same as the upstream stagnation pressure distortion, the axial velocity at the rotor inlet will therefore be circumferentially uniform. This simplified description neglects the effect of upstream swirl, but more detailed analysis including that effect shows the same result: non-uniform rotor exit static pressure distributions can cancel out the effect of incoming stagnation pressure distortion and yield circumferentially uniform rotor inlet flow [4].

A favorable rotor exit static pressure distribution can be created using a non-uniform stator exit flow angle distribution (i.e., with a non-axisymmetric stator geometry). As an example, for linearized, two-dimensional, incompressible flow, a sinusoidal variation in stator exit flow angle generates a static pressure distribution that lags behind the flow angle non-uniformity by 90° in θ. The resulting rotor exit static pressure depends on the magnitude of the stator exit angle distortion, the axial distance between the rotor and stator, the rotor exit stagnation pressure distribution, and the non-uniform static pressure rise across the stator. Through choice of $\alpha_5(\theta)$, it is possible to achieve circumferentially uniform flow at the rotor for a given inlet distortion and rotor geometry.

Similar ideas can be applied to reduce rotor flow distortions in three-dimensional flow, although the relationship between non-axisymmetric stator geometry and rotor exit static pressure non-uniformity is complicated by the three-dimensional flow redistribution upstream of the stator. Figure 16 shows circumferential distributions, at 90% span, of rotor exit static pressure and rotor diffusion factor for (i) the baseline stage design, (ii) the close-spaced axisymmetric stator, and (iii) a non-axisymmetric stator geometry at the baseline axial location. The latter two designs result in reductions in rotor static exit pressure, relative to

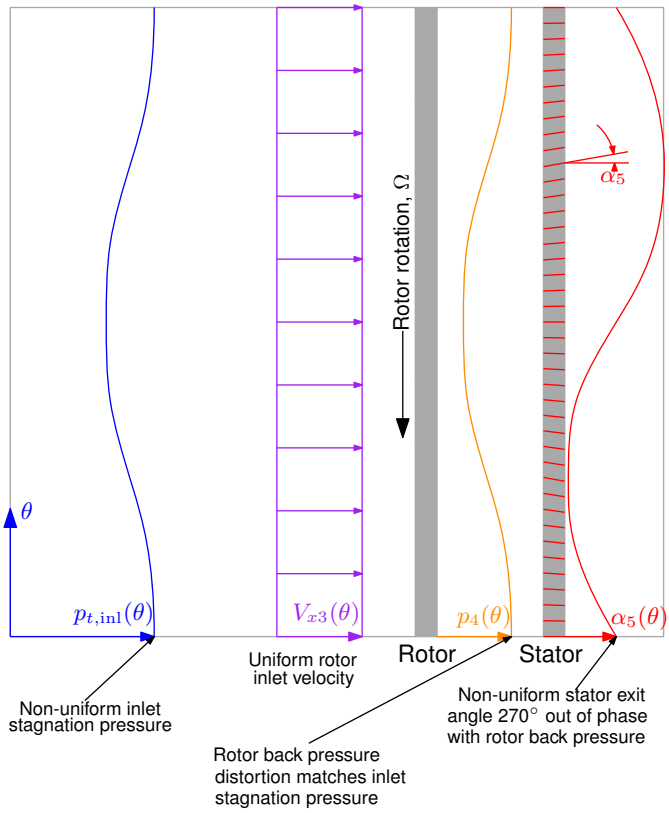

FIGURE 15. TWO-DIMENSIONAL APPROXIMATE FLOW MODEL FOR "UNROLLED" FAN STAGE SECTION WITH NON-AXISYMMETRIC STATOR DESIGN TO MITIGATE ROTOR INLET AXIAL VELOCITY DISTORTION

the baseline geometry, between approximately $\theta = 120°$ and $\theta = 240°$ where the peak diffusion occurs. The region of reduced rotor exit pressure increases the local acceleration through the rotor, alleviating the diffusion. Conversely, local increases in rotor exit pressure result in increases in local rotor diffusion. For the case considered, a 50% reduction in rotor diffusion facator distortion relative to the axisymmetric case was achieved with a stator exit angle non-uniformity of only 3°.

A favorable rotor exit static pressure non-unifomity can also be achieved with an axisymmetric stator by moving the stator upstream, closer to the rotor. With decreased rotor-stator spacing, the stator inlet swirl distortion, and thus stator static pressure rise distortion, increases. This reduces rotor exit static pressure near peak diffusion because the stator inlet axial velocity and stagnation pressure distortions are aligned, as seen in Fig. 9. This effect is weaker than the use of non-axisymmetric stators; the close-spaced stator (see Fig. 10) resulted in only a 10% reduction in rotor diffusion factor distortion relative to that observed with the baseline stator location.

The reduction in rotor diffusion factor distortion occurs in

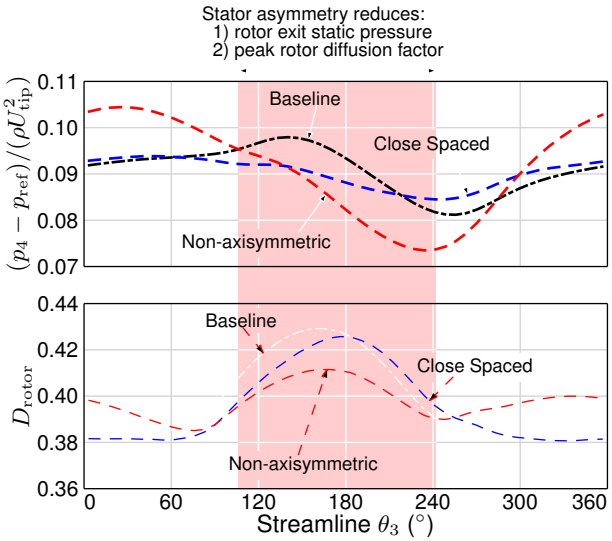

FIGURE 16. CIRCUMFERENTIAL DISTRIBUTIONS OF ROTOR EXIT PRESSURE AND DIFFUSION FACTOR AT 90% SPAN FOR BASELINE, CLOSE-SPACED, AND NON-AXISYMMETRIC ($\delta\kappa = 3°, \varphi_\kappa = 270°$) STATOR DESIGNS

part because of reduced attenuation of the upstream stagnation pressure distortion, resulting in increased axial velocity distortion downstream of the rotor and increased stator diffusion factor distortion. This explains the increased stator diffusion distortion seen in Fig. 14 for the close-spaced and non-axisymmetric stator designs, which reduce rotor diffusion distortion over a portion of the span. Moving the stator downstream decreases rotor-stator interaction. This leads to a less favorable rotor back pressure distortion, but it allows the radial redistribution in the rotor to continue farther downstream, reducing the stator inlet swirl distortion. For the geometry considered here, the distortion is also reduced due to annulus area contraction, and thus favorable pressure gradient, from rotor exit to stator inlet.

DISTORTION-TOLERANT BLI FAN DESIGN FEATURES

In this section, we discuss the insights gained into fan stage attributes to mitigate the effect of BLI inlet distortion, based on a metric of reduction in circumferential flow non-uniformity, specifically diffusion factor. Although we do not address the point further, it can be mentioned that such reductions can also lessen the unsteady forces on the rotor and the magnitude and duration of locally increased loading, which may impact stall margin [21].

Non-axisymmetric Stator Geometry

Changes in the rotor exit static pressure field via perturbations in stator exit flow angle were found to have the largest ef-

fect on rotor diffusion factor variation. Non-axisymmetric stator geometries can be used to mitigate the effect of flow non-uniformities due to downstream components (e.g., pylons) [27, 28], and they also appear to be well-suited to mitigate the effect of upstream non-uniformities due to BLI. Only circumferential variations in stator exit metal angle, as described by Eq. (10) were considered here. Different combinations of stator exit angle magnitude and phase produced reductions in rotor diffusion distortion at different spanwise locations, and we expect that a stator exit angle distribution with both radial and circumferential variations could generate a rotor exit pressure field that reduces rotor flow distortions over larger portions of the span. Such designs would reduce the rotor distortion attenuation and thus yield larger flow angle variations at the stator inlet, but that impact could be mitigated through non-axisymmetric tailoring of the stator leading edge to match the upstream flow angle.

Rotor Design Point Loading Distribution

The results of the analysis show the importance of both circumferential and radial redistribution effects in BLI created distortion. Cirumferential distortions in rotor incidence are largest near the hub, even though the stagnation pressure distortion far upstream is smallest for these streamlines. Distortions in rotor diffusion can be largest near midspan due to the combined effect of axial velocity and swirl non-uniformities. For a low loading design with steeper pressure rise characteristic slope, the upstream redistribution is stronger, and there is increased rotor inlet co- and counter-swirl. For the case examined, the largest decrease in rotor diffusion factor distortion occured at midspan for the high loading (shallow characteristic) design, and thus at higher average rotor diffusion factor. The implication is that there is a trade between average diffusion factor and diffusion factor distortion as the stage design point changes; it is not clear whether changes in overall stage loading can improve performance with BLI.

For a given stage design (stagnation enthalpy rise and flow coefficient), the three-dimensional flow redistribution is not sensitive to changes in the radial loading distribution. The local blade row response to changes in loading is similar to that seen in two-dimensional flows; increased loading leads to increased non-uniformity in the rotor and decreased non-uniformity in the stator, and this feature may be useful in affecting the local circumferential non-uniformities. For example, it may be beneficial to reduce the rotor tip loading, because non-uniformities in the tip region have been linked to reduction in fan stall margin [21]. Improvements in one performance at one spanwise section appear to worsen the performance at another location, however, and clear links between axisymmetric rotor loading distribution and overall performance improvments with BLI distortion are not yet defined.

SUMMARY AND CONCLUSIONS

A new, three-dimensional, throughflow method has been developed to evaluate, at the conceptual level (without the blade geometry needing to be defined), the response of fan stages to BLI inlet distortion. The turbomachinery is modeled using momentum and energy source distributions that are defined as a function of local flow conditions and a description of the blade mean camber surface. The method allows the estimation of flow fields using steady, inviscid CFD methods without a detailed blade geometry description. Comparison with higher fidelity methods shows the current method captures the principal features of non-uniform flow associated with fan response to BLI distortion.

Using the non-axisymmetric throughflow analysis, the impact of BLI inlet distortion on the fan stage flow field has been assessed. The results illustrate the importance of flow redistribution effects upstream and through the rotor. Some aspects of the distortion attenuation can be explained using ideas from two-dimensional distortion analysis, but a three-dimensional description is required to define the redistribution and the interactions between spanwise stations that generate the non-uniformities in low hub-to-tip ratio fan stages.

The effect of (i) fan stage radial loading distribution, (ii) rotor-stator spacing, and (iii) non-axisymmetric stator exit flow angle on circumferential variations in blade row diffusion has been assessed. Axisymmetric design changes result in tradeoffs between distortions in the rotor and stator or between spanwise sections of a given blade row. Non-axisymmetric stator exit flow angles, on the other hand, may be used to create favorable rotor exit static pressure distributions to reduce circumferential distortions in the rotor. Non-axisymmetric stator leading edge metal angles may be used to mitigate the effect of stator inlet distortion. Of the approaches examined, non-axisymmetric stator design appears to be best suited to improving BLI fan performance.

ACKNOWLEDGMENT

This research was sponsored by the Fundamental Aeronautics Program at the NASA Glenn Research Center under Cooperative Agreement Number NNX08AW63A, and the SUTD-MIT Graduate Fellows Program. The authors would also like to acknowledge E. J. Gunn, D. Perovic, and C. A. Hall of the Whittle Lab for information about their rig and measurements, and E. Envia of NASA for information on the R4 fan stage. Thanks also to J. J. Defoe, C. Lettieri, W. A. Sorensen, A. P. Kottapalli, M. L. Brand, and A. Peters for useful conversations during the development of the source term model, and M. Drela, N. A. Cumpsty, Z. S. Spakovszky, and A. Uranga for their helpful comments and suggestions.

NOMENCLATURE

A Area
AR Blade aspect ratio
B Number of blades
c Chord length
D Diffusion factor
$\dot{e}$ Specific energy source term
$\mathbf{f}$ Specific momentum source vector
f_ℓ Relative streamwise-parallel specific momentum source
f_n Relative streamwise-normal specific momentum source
h_t Stagnation enthalpy
$\dot{m}$ Mass flow
$\hat{\mathbf{n}}$ Blade camber surface normal
p Static pressure
p_t Stagnation pressure
s Entropy
U Wheel speed, $= \Omega r$
$\mathbf{V}$ Velocity vector
V Velocity magnitude
$\mathbf{W}$ Blade-relative velocity vector, $= \mathbf{V} - (\Omega r)\hat{\theta}$
W Blade-relative velocity magnitude
x, y, z Cartesian coordinate axes
x, r, θ Cylindrical coordinate axes
α Absolute swirl angle
β Reduce frequency, blade-relative swirl angle
δ Local relative flow deviation angle
$\delta\kappa$ Periodic stator exit angle non-uniformity magnitude
κ_{stator} Stator exit angle
ξ Stagger angle
ρ Density
ϕ Flow coefficient, $= V_{x3}/U_{\text{tip}}$
φ_κ Periodic stator exit angle non-uniformity phase
ψ Stagnation enthalpy rise coefficient, $= (h_{t4} - h_{t3})/U_{\text{tip}}^2$
Ω Wheel angular velocity

Subscripts

1 Far upstream measurement location
2 Fan inlet plane measurement location
3 Rotor inlet measurement location
4 Rotor exit/stator inlet interface measurement location
5 Stator exit measurement location
hub Blade hub
mid Blade midspan
ref Reference value
tip Blade tip

REFERENCES

[1] Betz, A., 1966. *Introduction to the Theory of Flow Machines*. Pergamon Press.

[2] Smith, L. H., 1993. "Wake Ingestion Propulsion Benefit". *Journal of Propulsion and Power,* ***9***, Jan.–Feb., pp. 74–82.

[3] Sato, S., 2012. "The Power Balance Method for Aerodynamic Performance Assesssment". PhD Thesis, Massachusetts Institute of Technology, Cambridge, MA, June.

[4] Hall, D. K., 2015. "Analysis of Civil Aircraft Propulsors with Boundary Layer Ingestion". PhD Thesis, Massachusetts Institute of Technology, Cambridge, MA, February.

[5] Hall, C. A., Schwartz, E., and Hileman, J. I., 2009. "Assessment of Technologies for the Silent Aircraft Initiative". *Journal of Propulsion and Power,* ***25***(6), pp. 1153–1162.

[6] Greitzer, E. M., Bonnefoy, P., De la Rosa Blanco, E., Dorbian, C., Drela, M., Hall, D., Hansman, R., Hileman, J., Liebeck, R., Lovergren, J., Mody, P., Pertuze, J., Sato, S., Spakovszky, Z., Tan, C., Hollman, J., Duda, J., Fitzgerald, N., Houghton, J., Kerrebrock, J., Kiwada, G., Kordonowy, D., Parrish, J., Tylko, J., and Wen, E., 2010. "N+3 aircraft concept designs and trade studies, Final Report". In NASA CR 2010-216794.

[7] Drela, M., 2011. "Development of the D8 Transport Configuration". In Proceedings of 29th AIAA Applied Aerodynamics Conference, Honolulu, HI, AIAA Paper 2011-3970, 27-30 June 2011.

[8] Uranga, A., Drela, M., Greitzer, E. M., Titchener, N. A., Lieu, M. K., Siu, N. M., Huang, A. C., Gatlin, G. M., and Hannon, J. A., 2014. "Preliminary Experimental Assessment of the Boundary Layer Ingestion Benefit for the D8 Aircraft". In Proceedings of 52th AIAA Aerospace Sciences Meeting, National Harbor, MD, pp. 13–17.

[9] Longley, J. P., and Greitzer, E. M., 1992. "Inlet Distortion Effects in Aircraft Propulsion System Integration". In *Steady and Transient Performance Prediction of Gas Turbine Engines*, Vol. 183 of *AGARD Lecture Series*. Chapter 7.

[10] Greitzer, E. M., and Griswold, H. R., 1976. "Compressor-Diffuser Interaction with Circumferential Flow Distortion". *Journal of Mechanical Engineering Science,* ***18***(1), pp. 25–38.

[11] Hynes, T., and Greitzer, E., 1987. "A Method for Assessing Effects of Circumferential Flow Distortion on Compressor Stability". *Journal of Turbomachinery,* ***109***(3), pp. 371–379.

[12] Florea, R. V., Matalanis, C., Hardin, L. W., Stucky, M., and Shabbir, A., 2015. "Parametric Analysis and Design for Embedded Engine Inlets". *Journal of Propulsion and Power*.

[13] Gunn, E. J., Tooze, S. E., Hall, C. A., and Colin, Y., 2013. "An Experimental Study of Loss Sources in a Fan Operating with Continuous Inlet Stagnation Pressure Distortion". *Joural of Turbomachinery,* ***135***(5), September, pp. 051002–051002–10. doi:10.1115/1.4007835.

[14] Gunn, E. J., and Hall, C. A., 2014. "Aerodynamics of Boundary Layer Ingesting Fans". In Proceedings of ASME Turbo Expo 2014: Turbine Technical Conference and Exposition, ASME. Paper number GT2014-26142.

[15] Defoe, J. J., and Hall, D. K., 2016. "Fan Performance Scaling with Inlet Distortions". In Proceedings of ASME Turbo Expo 2016: Turbine Technical Conference and Exposition, ASME. Paper number GT2016-58009.

[16] Marble, F., 1964. "Three-Dimensional Flow in Turbomachines". *High Speed Aerodynamics and Jet Propulsion,* ***10***, pp. 83–166.

[17] Gong, Y., Tan, C., Gordon, K., and Greitzer, E., 1999. "A Computational Model for Short-Wavelength Stall Inception and Development in Multi-stage Compressors". *Journal of Turbomachinery,* ***121***(4), pp. 726–734.

[18] Peters, A., Spakovszky, Z. S., Lord, W. K., and Rose, B., 2015. "Ultrashort Nacelles for Low Fan Pressure Ratio Propulsors". *Journal of Turbomachinery,* ***137***(2), p. 021001.

[19] Defoe, J. J., and Spakovszky, Z. S., 2013. "Effects of Boundary-Layer Ingestion on the Aero-Acoustics of Transonic Fan Rotors". *Journal of Turbomachinery,* ***135***(5), p. 051013.

[20] Horlock, J., 1971. "On Entropy Production in Adiabatic Flow in Turbomachines". *Journal of Fluids Engineering,* ***93***(4), pp. 587–593.

[21] Perovic, D., Hall, C. A., and Gunn, E. J., 2015. "Stall Inception in a Boundary Layer Ingesting Fan". In Proceedings of ASME Turbo Expo 2015: Turbine Technical Conference and Exposition, ASME. Paper number GT2015-43025.

[22] Hall, C. A., 2015. personal communication, 26 April.

[23] Pointwise®, Release 17, Pointwise User Manual, Pointwise, Inc., 2015.

[24] ANSYS® CFX, Release 16.2, ANSYS CFX-Solver Theory Guide, ANSYS, Inc.

[25] Hughes, C. E., 2002. "Aerodynamic Performance of Scale-Model Turbofan Outlet Guide Vanes Designed for Low Noise". In Proceedings of 40th AIAA Aerospace Sciences Meeting and Exhibit, AIAA. Paper number AIAA-2002-0374.

[26] Pandya, S. A., Espitia, A., and Uranga, A., 2014. "Computational Assessment of the Boundary Layer Ingesting Nacelle Design of the D8 Aircraft". In 52th AIAA Aerospace Sciences Meeting, National Harbor, MD, pp. 13–17.

[27] Kodama, H., and Nagano, S., 1989. "Potential Pressure Field by Stator/Downstream Strut Interaction". *Journal of Turbomachinery,* ***111***(2), pp. 197–203.

[28] Parry, A. B., 1996. "Optimisation of Bypass Fan Outlet Guide Vanes". In ASME 1996 International Gas Turbine and Aeroengine Congress and Exhibition, ASME. Paper number 96-GT-433.